PNAS RESEARCH ARTICLE | NEUROSCIENCE

Impairment of serine transport across the blood–brain barrier by deletion of Slc38a5 causes developmental delay and motor dysfunction

Inna Radzishevsky[a,1], Maali Odeh[a], Oded Bodner[a], Salman Zubedat[b], Lihi Shaulov[c], Maxim Litvak[a], Kayoko Esaki[d], Takeo Yoshikawa[e], Bella Agranovich[f], Wen-Hong Li[g], Alex Radzishevsky[h], Eyal Gottlieb[i], Avi Avital[b], and Herman Wolosker[a,f,1]

Edited by Reinhard Jahn, Max Planck Institute for Multidisciplinary Science, Goettingen, Germany; received February 17, 2023; accepted September 8, 2023

Brain L-serine is critical for neurodevelopment and is thought to be synthesized solely from glucose. In contrast, we found that the influx of L-serine across the blood–brain barrier (BBB) is essential for brain development. We identified the endothelial Slc38a5, previously thought to be a glutamine transporter, as an L-serine transporter expressed at the BBB in early postnatal life. Young Slc38a5 knockout (KO) mice exhibit developmental alterations and a decrease in brain L-serine and D-serine, without changes in serum or liver amino acids. Slc38a5-KO brains exhibit accumulation of neurotoxic deoxysphingolipids, synaptic and mitochondrial abnormalities, and decreased neurogenesis at the dentate gyrus. Slc38a5-KO pups exhibit motor impairments that are affected by the administration of L-serine at concentrations that replenish the serine pool in the brain. Our results highlight a critical role of Slc38a5 in supplying L-serine via the BBB for proper brain development.

D-serine | deoxysphingolipids | serine metabolism | synaptopathy

L-serine is important for the production of key metabolites and plays a role in several cellular processes, including sphingolipid production, folic acid cycle, and protein synthesis (1). L-serine also acts as a trophic factor that promotes neuronal survival and dendritogenesis (2). Brain L-serine is synthesized in astrocytes from glucose through the phosphorylated pathway by the sequential reactions of three enzymes: 3-phosphoglycerate dehydrogenase (Phgdh), phosphoserine aminotransferase (Psat1), and phosphoserine phosphatase (Psph) (1). Loss-of-function mutations in any of these enzymes lead to intellectual disability and microcephaly in children, along with a reduction in the CSF serine (1). Similarly, mutations in the L-serine transporter Slc1a4 promote intellectual disability, motor impairment, and postnatal microcephaly (3).

Astrocytic L-serine is exported to neurons in a process known as the serine shuttle (4), where it is converted to D-serine by the neuronal serine racemase (5). D-serine is a physiological coagonist of N-methyl-D-aspartate receptors (NMDARs) and is required for synaptic plasticity and learning and memory (6).

L-serine is often indispensable to cells with high metabolic rate (7). Brain metastases are particularly sensitive to inhibition of the serine synthesis pathway (7). Like cancer cells, the developing brain exhibits fast growth and high metabolic requirements (8). However, it is not known how the developing brain adjusts its metabolic requirements for serine.

The influx of L-serine from the blood into the brain occurs through the blood–brain barrier (BBB), a specialized structure composed of endothelial cells connected by junctions that prevent paracellular transport of substances (9). We now found that young mice import blood L-serine through the BBB at a rate 10-fold higher than older mice, suggesting that the blood is an important source of serine during development. We identified Slc38a5 as a brain microvessel-specific transporter that transports L-serine through the BBB in the early postnatal period. Slc38a5-KO mice show lower L- and D-serine levels in the brain during the first two postnatal weeks, along with metabolic, synaptic, and mitochondrial abnormalities and motor impairments. Our data suggest that the supply of blood L-serine through Slc38a5 is essential for early postnatal neurodevelopment.

Results

Young Mice Display Higher Influx of L-serine through the BBB. We evaluated the serine metabolism in mice at two different ages (P11 and P42) by administering stable-isotopes i.p. and subsequently measuring the synthesis of Ser$^{13}C_3$ from glucose$^{13}C_6$ and the uptake of Ser$^{13}C_1{}^{15}N$ into the brain (Fig. 1*A*). To minimize peripheral conversion of serine into glycine, mice were treated with Shin1 (Fig. 1*A*), an inhibitor of the serine hydroxymethyl

Significance

Previous studies assumed that all serine in the brain came exclusively from glycolysis, without any contribution from blood serine. Contrary to prevailing dogma, our research indicates that an additional supply of serine from the blood plays a critical role in postnatal brain development. We have identified Scl38a5 as a major L-serine transporter at the BBB that is critical for the influx of L-serine from the blood into the brain in the early postnatal period. Deletion of Slc38a5 leads to developmental delay, behavioral impairments, accumulation of deoxysphingolipids, and abnormal synapses and damaged mitochondria. Our observations suggest a unique metabolic pathway that is critical for early postnatal brain development and has implications for the pathology of serine deficiency syndromes.

Author contributions: I.R. and H.W. designed research; I.R., M.O., O.B., and H.W. performed research; I.R., S.Z., L.S., M.L., K.E., T.Y., B.A., W.-H.L., A.R., E.G., A.A., and H.W. contributed new reagents/analytic tools; I.R., O.B., A.R., and H.W. analyzed data; and I.R. and H.W. wrote the paper.

Competing interest statement: H.W. is in the advisory board of Spirify Pharma. A.R. owns Sonoworx Company.

This article is a PNAS Direct Submission.

[1]To whom correspondence may be addressed. Email: vinna@technion.ac.il or hwoloske@technion.ac.il.

This article contains supporting information online at https://www.pnas.org/lookup/suppl/doi:10.1073/pnas.2302780120/-/DCSupplemental.

Published October 9, 2023.

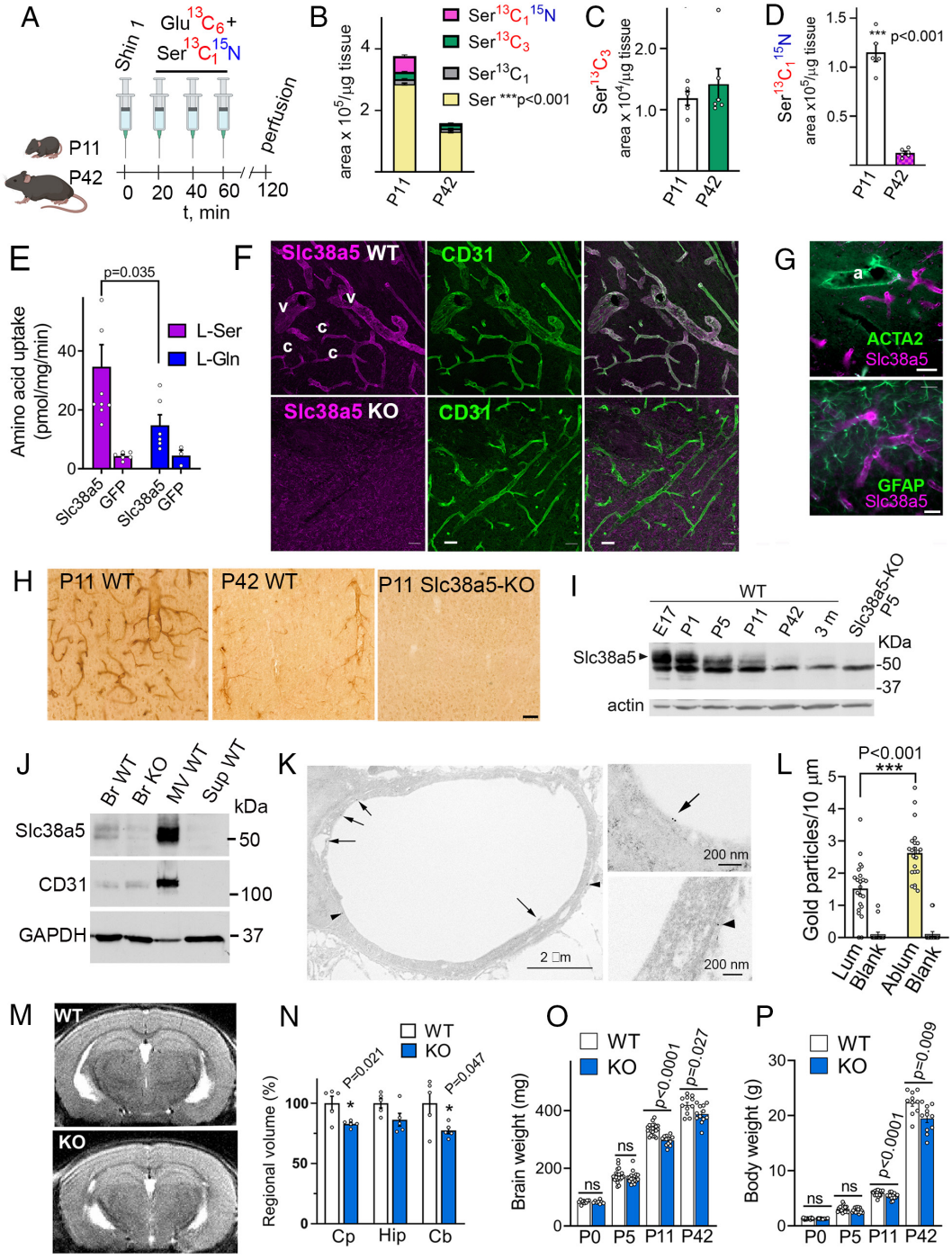

Fig. 1. Endothelial Slc38a5 is a serine transporter that plays a crucial role in postnatal brain growth. (*A*) Diagram of the experimental approach used in *B*–*D*. Young (P11) and older (P42) mice were injected with 50 mg/kg Shin1 (i.p.) followed by a mix of $Ser^{13}C_1{}^{15}N$ (50 mg/kg) and $glucose^{13}C_6$ (1 g/kg) every 20 min. Mice were transcardiacally perfused with ice-cold PBS and tissue were collected for LC-MS analysis. Data are mean ± SEM of 5 (P42) and 6 (P11) mice/group. (*B*) Serine isotopologue distribution in the hippocampus shows higher levels of unlabeled serine (Ser) and all ^{13}C-isotopologues in P11 mice when compared to P42 mice. Student's *t* test. (*C*) Synthesis of $Ser^{13}C_3$ in hippocampi of P11 and P42 mice from $glucose^{13}C_6$. The values were normalized by the serum $glucose^{13}C_6$ divided by unlabeled glucose. (*D*) Levels of $Ser^{13}C_1{}^{15}N$ in hippocampi of P11 and P42 mice, reflecting in vivo influx of blood $Ser^{13}C_1{}^{15}N$ into the brain. The values were normalized by the serum $Ser^{13}C_1{}^{15}N$ divided by the sum of all other serum serine isotopomers. Student's *t* test. (*E*) Slc38a5 exhibits a higher transport rate for L-[^{3}H]serine than L-[^{3}H]glutamine in HEK293 cells transfected with Slc38a5. Negative controls consisted of GFP-transfected cells. Data are mean ± SEM of 9 L-serine and 6 L-glutamine experiments. Student's *t* test. (*F*) Confocal image showing Slc38a5 expression in endothelial cells labeled by CD31 in the neocortex of P11 WT mice. Capillaries (c) were identified by a lumen size <10 µm and venules (v) by lumen size between 10 and 50 µm. The lower panels show lack of immunoreactivity in Slc38a5-KO mice tissue. (Scale bar, 50 µm.) (*G*) Slc38a5 is not expressed in arterioles (a) or astrocytes that are immunoreactive for Acta2 and GFAP, respectively. (*H*) Diaminobenzidine-peroxidase staining of Slc38a5 in the neocortex of WT mice show lower expression at P42 when compared to P11. The staining was absent in Slc38a5-KO mice. (Scale bar, 50 µm.) (*I*) Western blot of mouse cortical extracts shows high expression of Slc38a5 at embryonic day 17 (E17) and a progressive decline to undetectable levels in older ages. Control with Slc38a5-KO brain extract shows the specificity of the antibody. (*J*) Slc38a5 enrichment in brain microvessels of P1 mice. Br, brain; MV, purified microvessels; Sup, MV-depleted supernatant fraction. (*K* and *L*) Post-embedding electron microscopy. (*K*) Slc38a5 labeled by colloidal gold at the luminal (arrows) and abluminal (arrowheads) membrane of endothelial cells of the neocortex of P11 mice. Quantification of the gold particles (*L*) at the abluminal and luminal membranes. Student's *t* test. (*M*) T2-weighted MRI scans of P42 WT and Slc385-KO mice. (*N*) Regional volume reductions in brain regions. Cp, caudate putamen (striatum); Hip, hippocampus; Cb, cerebellum. Data are mean ± SEM of 5 mice/group. Student's *t* test. (*O*) Brain and (*P*) body weight of WT and Slc38a5-KO mice determined at different ages. Data are mean ± SEM of WT = 22, KO = 16 (P0); WT = 19, KO = 17 (P5); WT = 22, KO = 13 (P11); WT = 10, KO = 11 (P42) mice/group. Student's *t* test with Welch correction.

transferase 1 and 2 (10). As a control, we found that Shin1 does not cross the BBB (*SI Appendix*, Fig. S1*A*), but it increases serum L-serine levels in vivo (*SI Appendix*, Fig. S1*B*).

P11 mice have twice as much endogenous serine (Fig. 1*B*, yellow bar, $P < 0.001$) and increased $Ser^{13}C_1{}^{15}N$ (Fig. 1*B*, magenta bar) in the hippocampus compared to P42 mice. We found that the de novo synthesis of serine, as measured by the formation of $Ser^{13}C_3$ from glucose$^{13}C_6$, was the same in both young and older mice brains (Fig. 1*C*). Remarkably, P11 mice display a 10-fold higher influx of $Ser^{13}C_1{}^{15}N$ from the blood into the hippocampus when compared to P42 mice (Fig. 1*D*), indicating a higher permeability of the BBB to serine at young age. We confirmed that the higher levels of brain serine in P11 mice were not due to interconversion of serine and glycine, as the ratio of $Gly^{13}C_1{}^{15}N$ to $Ser^{13}C_1{}^{15}N$ was unaltered (*SI Appendix*, Fig. S1*C*).

Slc38a5 Transporter Uses L-serine as Substrate and Is Expressed in Brain Endothelial Cells. We investigated the potential reason for the higher influx of blood L-serine into young mice brains. Through analyzing transcriptome data (11), we noticed up to 100-fold enrichment of the Slc38a5 transporter in brain endothelial cells in comparison to other neural cells or peripheral vessels. While previous research has indicated that Slc38a5 functions as a glutamine and glycine transporter (12, 13), we found that Slc38a5 is much more efficient in transporting L-serine (Fig. 1*E*). The Km for L-serine (200 μM) is fivefold lower than for L-glutamine (*SI Appendix*, Fig. S2 *A* and *B*) and more than 10-fold lower than for D-serine and glycine (*SI Appendix*, Fig. S2 *C* and *D*).

We found that young mice (P11) robustly express the Scl38a5 transporter in CD31 (PECAM-1)-positive brain capillaries and venules (Fig. 1 *F*, *Top*). We confirmed the specificity of the Slc38a5 antibody by the lack of immunoreactivity in a constitutive Slc38a5-KO mice model (Fig. 1 *F*, *Lower*). No expression of Slc38a5 was detected in arterioles or astrocytes, identified by Acta2 and GFAP, respectively (Fig. 1*G*). The vascular staining for Slc38a5 was more widespread and robust in young (P11) than older (P42) mice, particularly in small capillaries (Fig. 1 *H*, *Left* and *Middle*). Western blot analysis of Slc38a5 revealed higher expression in perinatal ages, with a subsequent decrease in older mice to undetectable levels (Fig. 1*I*). Early expression of Slc38a5 in brain microvessels of E17 embryos was confirmed by immunostaining (*SI Appendix*, Fig. S3*A*). In agreement with the immunohistochemical localization of Slc38a5 in endothelial cells, we found a remarkable enrichment of Slc38a5 in purified brain microvessel fraction (Fig. 1*J*).

To determine the subcellular distribution of Slc38a5 in endothelial cells, we conducted electron microscopy and found that Slc38a5 is present in both the abluminal (brain-facing) and luminal (blood-facing) membranes (Fig. 1*K*). Slc38a5 is asymmetrically expressed, with more gold particles labeling the abluminal membrane (Fig. 1*L*).

Slc38a5-KO Mice Display Developmental Alterations. Deletion of the Slc38a5 gene affected postnatal brain growth. MRI indicates that Slc38a5-KO mice had a 20% reduction in the volumes of the striatum, hippocampus, and cerebellum (Fig. 1 *M* and *N*). Despite maintaining normal brain and body weight until P5, the Slc38a5-KO mice exhibited decreased brain and body weight at older ages (Fig. 1 *O* and *P*). The body-to-weight ratio was unchanged, indicating that both were equally affected (*SI Appendix*, Fig. S3*B*). Examination of the hippocampus and neocortex through Nissl staining revealed no gross abnormalities and similar number of Nissl bodies in the Slc38a5-KO mice (*SI Appendix*, Fig. S3*C*). GFAP expression was the same in WT and Slc38a5-KO mice, indicating lack of significant astrogliosis (*SI Appendix*, Fig. S3*D*). There were no changes in the phosphorylation of proteins involved in translation regulation, such as Akt, p70S6, 4EBP1, eIF2α, and others (*SI Appendix*, Fig. S3*E*). We used only males in the above tests and in subsequent studies. Because Slc38a5 is X-linked, controls for homozygous females would be from a different breeding pair and not from littermates. Furthermore, Slc38a5 escapes silencing of the paternal X chromosome in 30% of cases and is more expressed in female placental samples than in male samples, complicating the use of female mice (14).

Slc38a5 Controls Brain Serine Levels. To determine the impact of Slc38a5 deletion on amino acid substrates in vivo, we analyzed the brain levels of L-serine, D-serine, L-glutamine, and other amino acids in Slc38a5-KO mice and WT littermates by HPLC (Fig. 2 *A*–*C*). At P0 age, levels of L- and D-serine were not altered in Slc38a5-KO mice but were significantly decreased by P5 and P11 (Fig. 2 *A* and *B*). Notably, in P42 mice, which express little to no Slc38a5 (Fig. 1 *H* and *I*), there were no differences in serine enantiomer levels between Slc38a5-KO mice and WT littermates (Fig. 2 *A* and *B*).

No differences were observed in brain L-glutamine content at any age (Fig. 2*C*), indicating that Slc38a5 does not control brain glutamine levels. Furthermore, HPLC analysis did not reveal changes in other potential Slc38a5 substrates in the brain (Fig. 2*D*).

Lower levels of serine in Slc38a5-KO mice were not due to changes in serine metabolic enzymes. The expression of Phgdh and PSAT1 was unchanged in the brains of young Slc38a5-KO mice (Fig. 2*E*). Serine racemase, which converts L-serine to D-serine (5) as well as glutamine synthetase were also unaltered (Fig. 2*E*).

Next, we carried out targeted metabolomics of four brain regions as well as serum and liver (*SI Appendix*, Tables S1–S6). In order to mitigate false positives and exclude biologically irrelevant changes, we examined metabolites that exhibited alterations in at least three brain regions and displayed a minimum change of 10%. We confirmed a reduction in serine levels across all four brain regions in the Slc38a5-KO mice (*SI Appendix*, Fig. S4*A*). We also found a decrease in threonine levels in all brain regions of Slc38a5-KO mice (*SI Appendix*, Fig. S4*B*), whereas 2-phosphoglycerate (P2G) increased in three brain regions (*SI Appendix*, Fig. S4*C*). There were no differences between the hippocampus and other brain regions regarding serine, threonine, or P2G levels (*SI Appendix*, Fig. S4 *A*–*C*, *Right*). Some metabolites were not pursued as they were not consistently different than WT in more than 2 brain regions or changed less than 10%. (*SI Appendix*, Tables S1–S4). Moreover, no changes were detected in the serum or liver for any of the metabolites at FDR<0.1 (*SI Appendix*, Fig S4*D* and Tables S5 and S6).

Because threonine is decreased in the brains of Slc38a5-KO mice, we investigated whether threonine is a substrate of Slc38a5. We found that the transport of L-[^{3}H]threonine by ectopically expressed Slc38a5 was five times lower than that of L-[^{3}H]serine (*SI Appendix*, Fig. S4*E*). In addition, the serum concentration of serine is twice that of threonine (*SI Appendix*, Fig. S4*F*), indicating that threonine is probably not a physiological substrate for Slc38a5.

Transport of Serine Enantiomers In Vivo by Slc38a5 at the BBB. We monitored the Slc38a5-mediated transport at the BBB in vivo by injecting radiolabeled amino acids intracardiacally (Fig. 3*A*). We measured the extraction fraction (EF) of each amino acid from the blood into the brain relative to the EF of L-glutamate that was coinjected along with amino acids of interest. L-Glutamate is not a substrate of Slc38a5 and its EF was used to normalize the values to

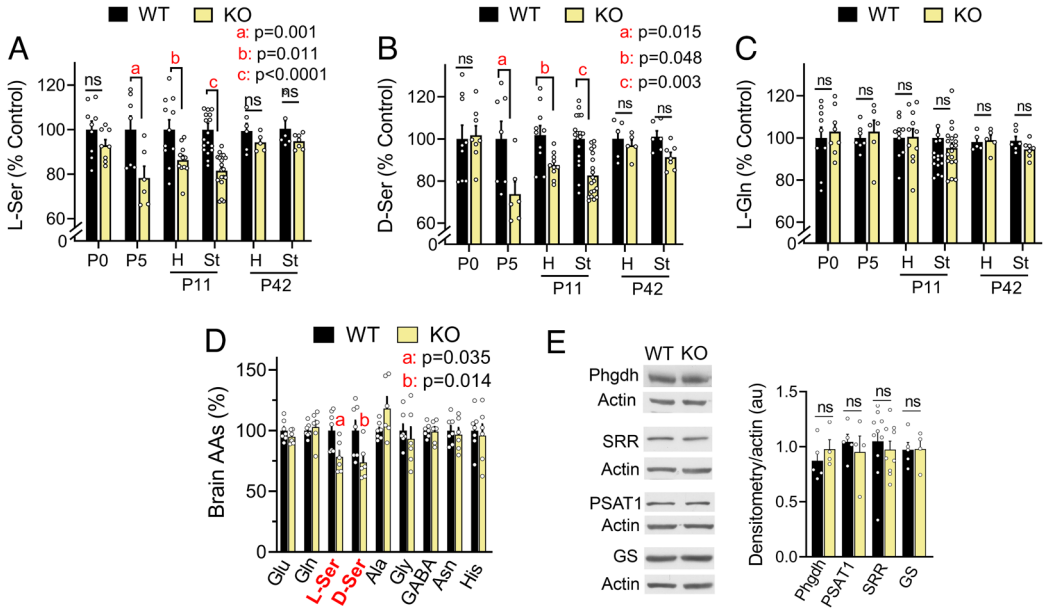

Fig. 2. Slc38a5 regulates brain serine levels during the first two postnatal weeks without altering serum amino acid levels. Age-dependent change in L-serine (*A*), D-serine (*B*), and L-glutamine (*C*) in P0–P42 mice monitored by HPLC. H, hippocampus; St, striatum. One-way ANOVA and Holm-Sidak multiple comparisons test (P0, WT = 9 and KO = 8 mice; P5, WT = 7 and KO = 6; P11 (St), WT = 17 and KO = 19; P11 (H), WT = 11 and KO = 11; P42 (St), WT = 6 and KO = 7; P42 (H), WT = 6 and KO = 5). (*D*) Selective decrease in serine enantiomers in Slc38a5-KO mice brains (P5) compared to other amino acids. The *P* values were adjusted using the two-stage step-up false discovery method of Benjamini, Krieger, and Yekutieli. The data for L-Ser and D-Ser levels were replotted from panels *A* and *B* (P5) for comparison with other brain amino acids. (*E*) Western blot of serine and glutamine metabolic enzymes and quantification of the expression normalized for actin. Phgdh, 3-phosphoglycerate dehydrogenase; SRR, serine racemase; PSAT1, phosphoserine aminotransferase 1; GS, glutamine synthetase in the striatum of P11 mice. Data represent the mean ± SEM of 4 to 10 mice/group.

account for changes in cardiac output among the mice. We found that young Slc38a5-KO mice exhibit lower in vivo BBB transport of three substrates: L-serine, D-serine, and L-glutamine (Fig. 3 *B–D*). In vivo uptake of L-threonine (Fig. 3*E*) or glycine (Fig. 3*F*) was not affected in Slc38a5-KO mice, indicating that they are not physiologic substrates for Slc38a5 at the BBB. We also performed controls, such as coinjecting L-serine with 3-O-methyl-D-glucose (3OMG), which confirmed the decrease in L-serine transport via the BBB in young Slc38a5-KO mice (Fig. 3*G*).

Leucine uptake was not affected in Slc38a5-KO mice (Fig. 3*H*), suggesting that there is no functional change in system L transporters (e.g., Slc7a5, Slc7a8), which use leucine as substrate (9). As an additional control, we monitored the EF of amino acids in the kidneys, which do not express Slc38a5 (15). The uptake of all tested amino acids was unaffected in the kidneys of Slc38a5-KO mice (*SI Appendix*, Fig. S6 *A–H*).

A recent study found that knockdown of Slc38a5 delays retinal vessel development (16). We did not detect any change in

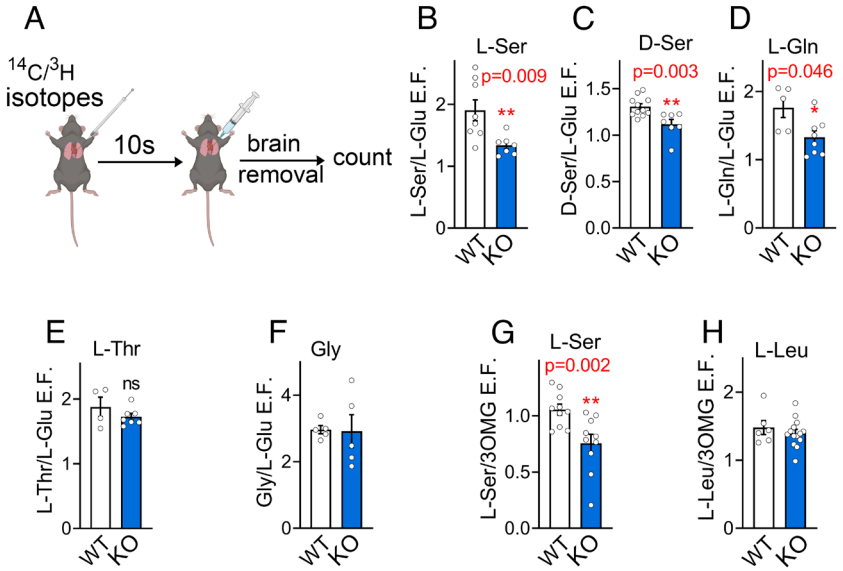

Fig. 3. Slc38a5-KO mice exhibit decreased serine transport through the BBB. (*A*) Diagram of the experimental approach used for determining the extraction fraction (EF) of amino acids from the blood into the brain in P11-13 mice. (*B*) Ratio of L-[^{3}H]serine and L-[^{14}C]glutamate EFs (8 WT and 7 KO). (*C*) Ratio of D-[^{3}H]serine and L-[^{14}C]glutamate EFs (11 WT and 7 KO). (*D*) Ratio of L-[^{3}H]glutamine and L-[^{14}C]glutamate EFs (5 WT and 8 KO). (*E*) Ratio of L-[^{3}H]threonine and L-[^{14}C]glutamate EFs (4 WT and 7 KO). (*F*) Ratio of [^{14}C]glycine and L-[^{3}H]glutamate EFs (5 WT and 5 KO). (*G*) Ratio of L-[^{14}C]serine and 3-O-[Methyl-^{3}H]D-glucose (3OMG) EFs (10 WT and 10 KO). (*H*) Ratio of L-[^{14}C]leucine and [^{3}H]3OMG EFs (6 WT and 14 KO). Data are means ± SEM. Mann–Whitney *U* test (*A–H*).

microvessel density in Slc38a5-KO mice monitored by CD31 immunofluorescence (*SI Appendix*, Fig. S5*A*). Furthermore, BBB permeability for fluorescein (*SI Appendix*, Fig. S5*B*) or 10-kDa dextran (*SI Appendix*, Fig. S5*C*) was not altered in Slc38a5-KO mice, indicating that Slc38a5 deletion does not affect BBB permeability.

Slc38a5 Transporter Acutely Regulates Brain L-serine but Not L-glutamine Levels. To investigate the role of Slc38a5 in acutely regulating brain L-serine levels, we injected the mice with an excess of L-glutamine to compete with serum serine for transport through Slc38a5 (Fig. 4*A*). We found that L-glutamine administration acutely decreased the levels of brain L-serine (Fig. 4*A*) and D-serine (Fig. 4*B*) in WT but not in Slc38a5-KO mice. This suggests that Slc38a5 plays a role in regulating the steady-state levels of L-serine and D-serine in the brain. Conversely, we injected L-serine at concentrations that increased brain L-serine by 30% ± 8.5 (n = 8) and found that it does not affect the levels of L-glutamine (Fig. 4*C*) or its metabolite L-glutamate (Fig. 4*D*). Our observations indicate that L-glutamine transport by Slc38a5 appears to be negligible for maintaining brain L-glutamine levels but that blood glutamine levels can be an important regulator of brain serine levels.

Lower Transport of L-serine across the BBB of Slc38a5-KO Mice but Normal L-serine Synthesis. To examine L-serine transport via Slc38a5 and its synthesis from glucose, we coinjected Ser$^{13}C_1{}^{15}N$ with glucose$^{13}C_6$ in P11 WT and Slc38a5-KO mice. We found reduced L-Ser$^{13}C_1{}^{15}N$ influx into the hippocampus of Slc38a5-KO mice (25% decrease, P = 0.052) (Fig. 4*E*). No changes were observed in the liver Ser$^{13}C_1{}^{15}N$ (Fig. 4*F*). Furthermore, L-serine synthesis, as measured by the formation of Ser$^{13}C_3$ from glucose$^{13}C_6$, was unaffected in the hippocampus (Fig. 4*G*) and liver (Fig. 4*H*) of Slc38a5-KO mice. Conversion of serine into glycine, inferred by the formation of Gly$^{13}C_1{}^{15}N$ from Ser$^{13}C_1{}^{15}N$, was not altered in Slc38a5-KO mice as well (Fig. 4*I*). Overall, the data suggest that the lower brain L-serine levels in young Slc38a5-KO mice are due to a deficiency in L-serine import and not a change in de novo L-serine synthesis.

Accumulation of Neurotoxic Deoxysphingolipids in Slc38a5-KO Mice. We investigated whether deletion of Slc38a5 affects the sphingolipid pathway, which uses L-serine as a precursor to generate sphinganine through the condensation with palmitoyl-CoA catalyzed by serine palmitoyltransferase (SPT). Promiscuous condensation of palmitoyl-CoA with alanine or glycine by SPT results in the formation of highly toxic deoxysphingolipids (doxSLs), such as deoxysphinganine (doxSA), deoxymethylsphinganine (doxmeSA), and deoxydihydroceramide (doxDHCer) (see *SI Appendix*, Fig. S7 for structures) (17, 18). We found that P5 Slc38a5-KO mice had a 40% higher brain L-alanine/L-serine ratio but a normal glycine/L-serine ratio (Fig. 5*A*). We hypothesized that the higher

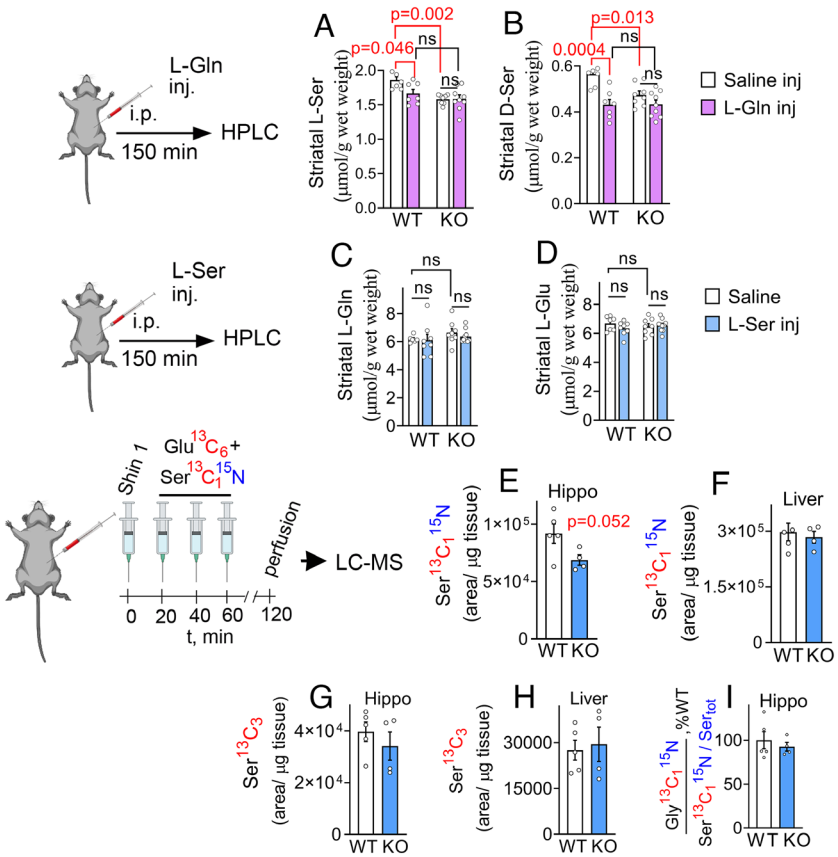

Fig. 4. Slc38a5 controls the steady-state levels of brain serine enantiomers independently of serine synthesis from glucose. (*A* and *B*) WT and Slc38a5-KO mice (P11–13) were injected i.p. with L-Gln (2 mmol/kg) and 2.5 h later, striatal levels of L-Ser and D-Ser were quantified. L-Gln injection caused a decrease in brain L-serine (*A*) and D-serine (*B*) in WT but not in Slc38a5-KO pups. One-way ANOVA and Sidak multiple comparisons test. (*C* and *D*) WT and Slc38a5-KO mice (P11–P13) were injected with L-serine (2 mmol/kg) and processed as described in A-B. Striatal levels of L-Gln (*C*) and L-Glu (*D*) were unaltered by L-Ser injection in both genotypes. (*E–I*) Serine metabolism in the brain and liver of WT and Slc38a5-KO mice (P11–P13). Animals were injected with Shin1 followed by a mix of Ser$^{13}C_1{}^{15}N$ (50 mg/kg) and glucose$^{13}C_6$ (1 g/kg). Ser$^{13}C_1{}^{15}N$ and Ser$^{13}C_3$ analyzed by LC-MS. Slc38a5-KO displayed a lower import of Ser$^{13}C_1{}^{15}N$ into the hippocampus (*E*) but not the liver (*F*). The values in *E* and *F* were normalized by the serum Ser$^{13}C_1{}^{15}N$ divided by the sum of all other serum serine isotopologues. There was no change in the synthesis of Ser$^{13}C_3$ from glucose$^{13}C_6$ in either the hippocampus (*G*) or liver (*H*) of Slc38a5-KO mice. The values of Ser$^{13}C_3$ in *G* and *H* were normalized by the serum glucose$^{13}C_6$ divided by the unlabeled glucose. (*I*) Conversion of Ser$^{13}C_1{}^{15}N$ into Gly$^{13}C_1{}^{15}N$ and was unaltered in the hippocampus of Slc38a5-KO mice. Hippo, hippocampus. Data are means ± SEM of 5 WT and 4 KO. Welch's *t* test.

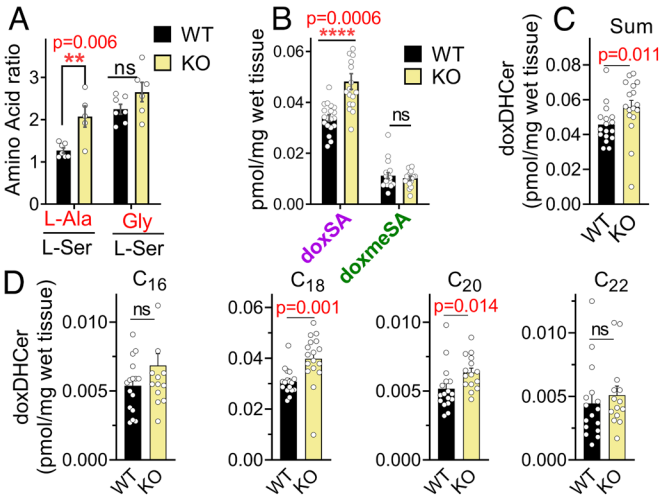

Fig. 5. Accumulation of atypical deoxysphingolipids in Slc38a5-KO mice. (*A*) Slc38a5-KO mice (P5) display higher L-Ala to L-Ser ratio in the brain, but normal Gly to L-Ser ratio. Data are means ± SEM of 7 WT and 5 KO mice. One-way ANOVA and Sidak multiple comparisons test. (*B*) Slc38a5-KO (P5) accumulates doxSA in the brain but not doxmeSA. Data are means ± SEM of 19 WT and 17 KO brains. Brown–Forsythe and Welch ANOVA and Dunnett's T3 multiple comparisons test. (*C*) Slc38a5-KO mice brains (P5) have higher levels of total doxDHCer species. (*D*) C_{18} and C_{20} were the main doxDHCer species that accumulated in the Slc38a5-KO mice. Mann–Whitney *U* test adjusted by Benjamini, Krieger, and Yekutieli FDR approach. Data are means ± SEM of 19 WT and 17 KO brains.

L-alanine/L-serine ratio in Slc38a5-KO mice leads to the formation of doxSLs by SPT. Using targeted LC-MS analysis, we found higher levels of doxSA (Fig. 5*B*) in the brains of P5 Slc38a5-KO mice. Deoxydihydroceramides (doxDHCer), which are downstream products of doxSA, were increased in the brains of P5 Slc38a5-KO mice (Fig. 5 *C* and *D*), mainly because of the increase in C_{18}-doxDHCer, the most abundant species. On the other hand, levels of normal sphingolipids (e.g., dihydroceramides, ceramides, lactosylceramides, hexosylceramides, and sphingomyelin) were not altered in P5 Slc38a5-KO mice (*SI Appendix*, Fig. S8).

Synaptic and Mitochondrial Abnormalities in Slc38a5-KO Mice. Deoxysphingolipids are neurotoxic and cause synapse damage and mitochondrial dysfunction (17, 18). We used electron microscopy to analyze the synapses and mitochondria in the molecular layer of the dentate gyrus (Fig. 6*A*), a region that has very active synaptogenesis at P4 to P11 (19). Asymmetric (excitatory) synapses from P11 Slc38a5-KO mice (Fig. 6*B*) contained shorter postsynaptic densities (Fig. 6*C*) and showed a significant decrease in postsynaptic density area (Fig. 6*D*). The distribution of postsynaptic density length and area were shifted toward lower values in the Slc38a5-KO mice (Fig. 6 *C* and *D*). The active zone, containing the release-ready and proximal vesicle pools, was smaller in Slc38a5-KO mice (Fig. 6*E*). Although the density of vesicles /nm^2 of active zone was unaltered (Fig. 6*F*), the number of vesicles/active zone (Fig. 6*G*) was lower due to the smaller area of the active zones in the Slc38a5-KO.

The number of asymmetric synapses in Slc38a5-KO mice remained unchanged (Fig. 6 *H*, *Left*), but we observed an increase in the number of symmetric synapses (Fig. 6 *H*, *Right*), which are generally considered inhibitory. The presynaptic bouton areas of both symmetric and asymmetric synapses in Slc38a5-KO mice were the same as in WT (*SI Appendix*, Fig S9 *A*–*C*).

We then analyzed mitochondrial morphology by quantifying mitochondria with degenerative changes, like electron-lucent swelling of the matrix, fragmentation of the cristae, and disruption of the outer membrane (Fig. 6*I*, arrowheads). Deletion of Slc38a5 resulted in a 4-fold increase in damaged mitochondria (Fig. 6*J*). This was associated with a several-fold increase in mitophagy-like events, such as phagophore formation and mitophagosome-like structures (Fig. 6*I*, red arrows, and Fig. 6*J*, *Middle*). Total number of mitochondria remained unchanged in Slc38a5-KO mice (Fig. 6 *J*, *Right*). We also detected higher levels of Rheb, a synaptic mitophagy initiator (20), and LC3BII, a protein involved in autophagosome formation, in brain mitochondrial fraction of Slc38a5-KO mice (Fig. 6*K*).

Reduced Hippocampal Neurogenesis in Slc38a5-KO Mice. Administration of D-serine increases cell proliferation and survival of new neurons in the adult hippocampus (21). Given the decrease in L-serine and D-serine in Slc38a5-KO mice, we examined cell proliferation and neurogenesis in the dentate gyrus, which has a high rate of neurogenesis in all layers at young age (22). Slc38a5-KO mice showed no changes in cell proliferation marker (Ki-67) (Fig. 7 *A* and *B*) or marker for neural stem cells and astrocytes (Sox-2) (Fig. 7 *A* and *C*). Injections of 5-ethyl-2'-deoxyuridine (EdU) at P5 mice, which is incorporated in the DNA of newly formed cells, revealed similar total numbers of new EdU+ cells between WT and Slc38a5-KO mice (Fig. 7*E*). No differences were observed in the generation of immature neurons, as the colocalization of EdU with doublecortin (DCX) was unchanged in the Slc38a5-KO mice (Fig. 7 *D*, *F*, and *G*). However, the number of mature neurons (EdU+/NeuN+ cells) was lower in Slc38a5-KO mice, indicating lower survival of newly formed neurons (Fig. 7 *D*, *G*, and *H*).

Why would a decrease in serine affect neuron survival and spare dividing cells? Neurons lack the enzymes required for de novo L-serine synthesis, such as Phgdh (5). However, we found that Phgdh is expressed in dividing cells positive for Ki-67 and Sox-2 in the dentate gyrus (Fig. 7*I*). In light of their dependence on externally supplied L-serine, newborn neurons in young brain appear to be a cell population particularly sensitive to a decrease in L-serine levels.

Slc38a5-KO Exhibit Enhanced Ultrasonic Vocalizations (USVs). To examine the impact of serine deficiency on mouse behavior, we studied motor and nonmotor phenotypes of Slc38a5-KO mice. We observed an increase in USVs in pups separated from their dams and littermates. Specifically, P9 and P10 mice showed a significant increase in call frequency (Fig. 8*A*). Such an increase in USVs is reminiscent of some models of autism spectrum disorders (9). The calls were also more complex, such as composite calls, while short calls tended to decrease (Fig. 8*B*).

Motor Impairments in Slc38a5-KO Mice. We evaluated motor coordination in mouse pups through various tasks. Slc38a5-KO mice (P5) exhibited normal righting reflex (Fig. 8*C*). Slc38a5-KO mice (P11) had a longer latency to turn in the negative geotaxis test, indicating motor coordination impairment (Fig. 8*D*). Slc38a5-KO mice also had weaker grip strength, as seen in the iron mesh inversion test (Fig. 8*E*). The latency to fall was shorter in the hindlimb (Fig. 8*F*) and upper-limb suspension tests (Fig. 8*G*), indicating further motor coordination deficits in Slc38a5-KO mice

We evaluated the role of serine deficiency in the behavioral abnormalities by perinatal administration of L-serine to the dam, which increases L-serine levels in the offspring's plasma (23). We took advantage of the fact that Slc38a5 is not the sole serine transporter at the BBB, as the deletion of Slc38a5 only reduces the overall brain serine influx by 30% (Fig. 3*B*). This means that supplying excessive L-serine should compensate for the loss of Slc38a5 and restore brain serine levels, thus improving the phenotype of Slc38a5-KO mouse pups. L-serine supplementation improved the motor coordination deficits seen in Slc38a5-KO offspring (P11) compared to WT in

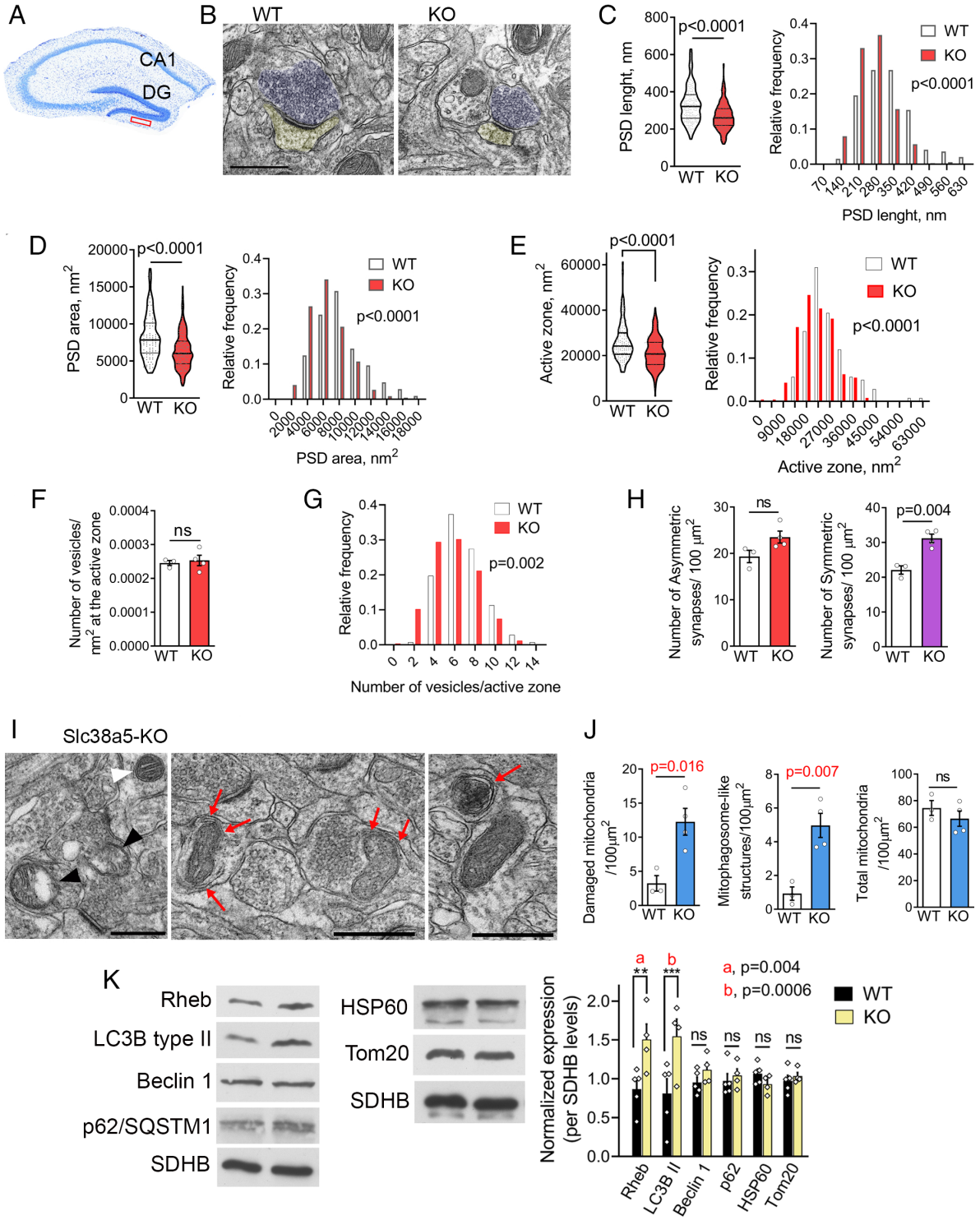

Fig. 6. Abnormal synapses and damaged mitochondria in young Slc38a5-KO mice. (*A*) Diagram of the ventral leaflet area of the dentate gyrus (DG) examined for synaptic and mitochondria morphology. (*B*) Representative electron micrographs of WT and Slc38a5-KO mice (P14) asymmetric synapses showing the presynapse (blue) in apposition to the postsynapse (yellow), which contains a postsynaptic density (PSD) and synaptic cleft. (Scale bar, 500 nm.) (*C*) Slc38a5-KO mice display shorter PSD length and a distribution toward lower length values. Data are from 255 (WT) and 432 (KO) synapses. Mann–Whitney test and Kolmogorov–Smirnov test for frequency distribution. (*D*) Slc38a5-KO mice exhibit a smaller PSD area and the distribution was skewed towards lower values. Data are from 165 (WT) and 377 (KO) synapses. Mann–Whitney *U* test and Kolmogorov–Smirnov test for frequency distribution. (*E*) The active zone area was smaller in the Slc38a5-KO mice. Data represents 142 and 256 active zones of 3WT and 4 KO mice, respectively. Mann–Whitney *U* test and Kolmogorov–Smirnov test for frequency distribution. (*F*) Number of vesicles at the active zone normalized by the area. Student's *t* test. (*G*) Slc38a5-KO display lower number of synaptic vesicles/active zone consisting of the proximal and release-ready pools. Statistics and mice numbers as in *E*. (*H*) Number of asymmetric synapses compared to symmetric synapses in WT and Slc38a5-KO mice. Data are from 3 (WT) and 4 (KO) mice. (*I*) Electron micrograph of Slc38a5-KO mice showing damaged mitochondria (black arrowheads) along with normal mitochondria (white arrowhead). *Middle* panel shows phagophores engulfing mitochondria to form the mitophagosome-like structures (red arrows). *Right* panel shows a fully formed mitophagosome-like structure containing a double membrane (red arrow). (Scale bar, 500 nm.) (*J*) Slc38a5-KO mice exhibit higher number of damaged mitochondria (left graph), more mitophagosome-like structures (middle graph), but unaltered number of mitochondria (WT = 3 mice, KO = 4 mice). Student's *t* test. (*K*) Western blot of brain mitochondrial fraction of P11 mice with mitochondrial and mitophagy/autophagy markers (5 WT and 4 KO mice). Graph on the right shows the quantification of the expression normalized by the mitochondrial marker succinate dehydrogenase B (SDHB). One-way ANOVA with Sidak's multiple comparisons correction.

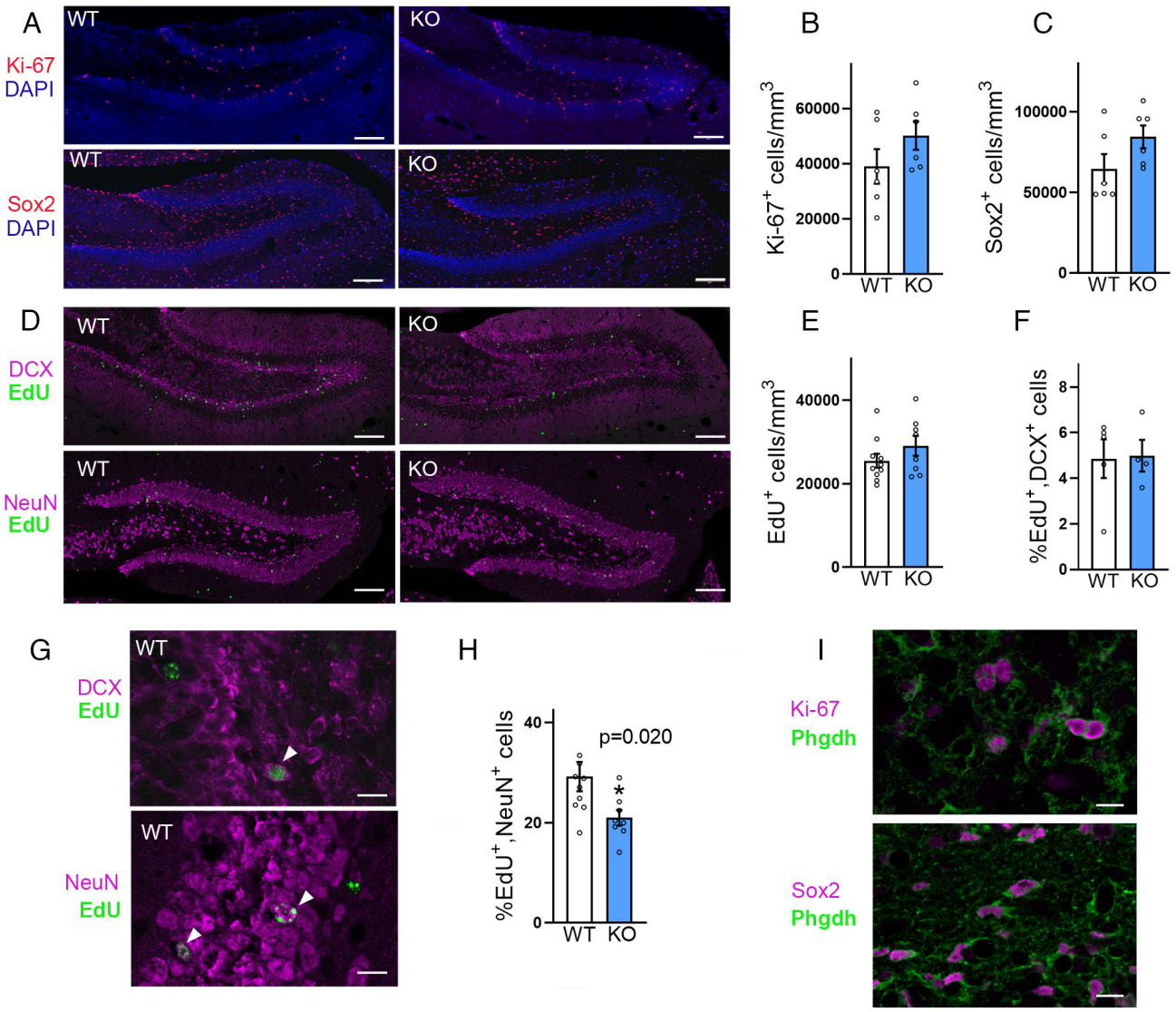

Fig. 7. Deletion of Slc38a5 decreases neuronal survival. (*A*) Confocal images of the dentate gyrus of P11 WT and Slc38a5-KO mice labeled for Ki67 and Sox2. (*B* and *C*) Quantification of cells labeled for Ki-67 (*B*, 6 mice/group), Sox2 (*C*, 6 mice/group) revealed no change in Slc38a5-KO mice. (*D*) Confocal images of the dentate gyrus of WT and Slc38a5-KO mice injected with 50 mg/kg EdU at P5 and examined for colocalization of EdU and doublecortin (DCX) or NeuN at P19. (Scale bar, 100 μm.) (*E* and *F*) Quantification of cells labeled for EdU (*E*) (9 WT and 7 Slc38a5-KO) and positive for both EdU and DCX (*F*) (5 WT and 4 Slc38a5-KO) revealed no change in Slc38a5-KO mice. (*G*) Confocal images of cells positive for both EdU and DCX or EdU and NeuN. (Scale bars, 5 μm.) (*H*) Slc38a5-KO mice exhibit a lower number of mature neurons, which are positive for both EdU and NeuN (*F*, 8 WT and n = 5 Slc38a5-KO). Student's *t* test. (*I*) Phgdh expression in Ki-67 and Sox2-expressing cells. (Scale bar, 5 μm.)

some but not all tests (Fig. 8 *D*–*G*, right columns). The brain and body weight differences between the genotypes disappeared after L-serine treatment (Fig. 8 *H* and *I*). While L-serine supplementation decreases food intake and body weight (23), it did not negatively affect Slc38a5-KO mice. The brain/body weight ratio of L-serine-treated WT was the same as that of L-serine-treated Slc38a5-KO and exceeded the brain/body weight of naive mice (Fig. 8*J*). However, it is unlikely that changes in body weight of the mouse pups underlie the motor improvement caused by L-serine administration. The body weight was not correlated with the performance of either WT or Slc38a5-KO mice pups in any of the motor tests used (*SI Appendix*, Fig. S10).

We confirmed that administration of L-serine increased its own levels in the hippocampus of Slc38a5-KO mice (Fig. 8*K*, $P < 0.001$). In contrast, we did not detect an increase in hippocampal D-serine (Fig. 8*L*) or threonine (Fig. 8*M*). The latter decreased even further with L-serine supplementation.

We also treated the dams perinatally with D-serine. We found that D-serine failed to improve motor coordination (*SI Appendix*, Fig. S11 *A*–*D*) or alter brain and body weight (*SI Appendix*, Fig S11 *E* and *F*). D-Serine treatment effectively increased its levels in the hippocampus of Slc38a5-KO mice (*SI Appendix*, Fig. S11*G*). Our data are compatible with the notion that the impaired supply of L-serine (but not D-serine or threonine) through the BBB causes developmental and motor deficits in Slc38a5-KO mice.

Discussion

We have discovered a new pathway regulating brain development that involves the influx of L-serine through the BBB by the Slc38a5 transporter in young mice. Contrary to the prevailing dogma, we found that de novo synthesis of serine from glucose is insufficient for early postnatal brain development. L-serine supply from the blood is essential for the production of D-serine, synaptic and mitochondrial homeostasis, neurogenesis, and sphingolipid metabolism. This blood–brain serine pathway is prominent in young mice as they perinatally express the endothelial Slc38a5 transporter (*SI Appendix*, Fig. S12).

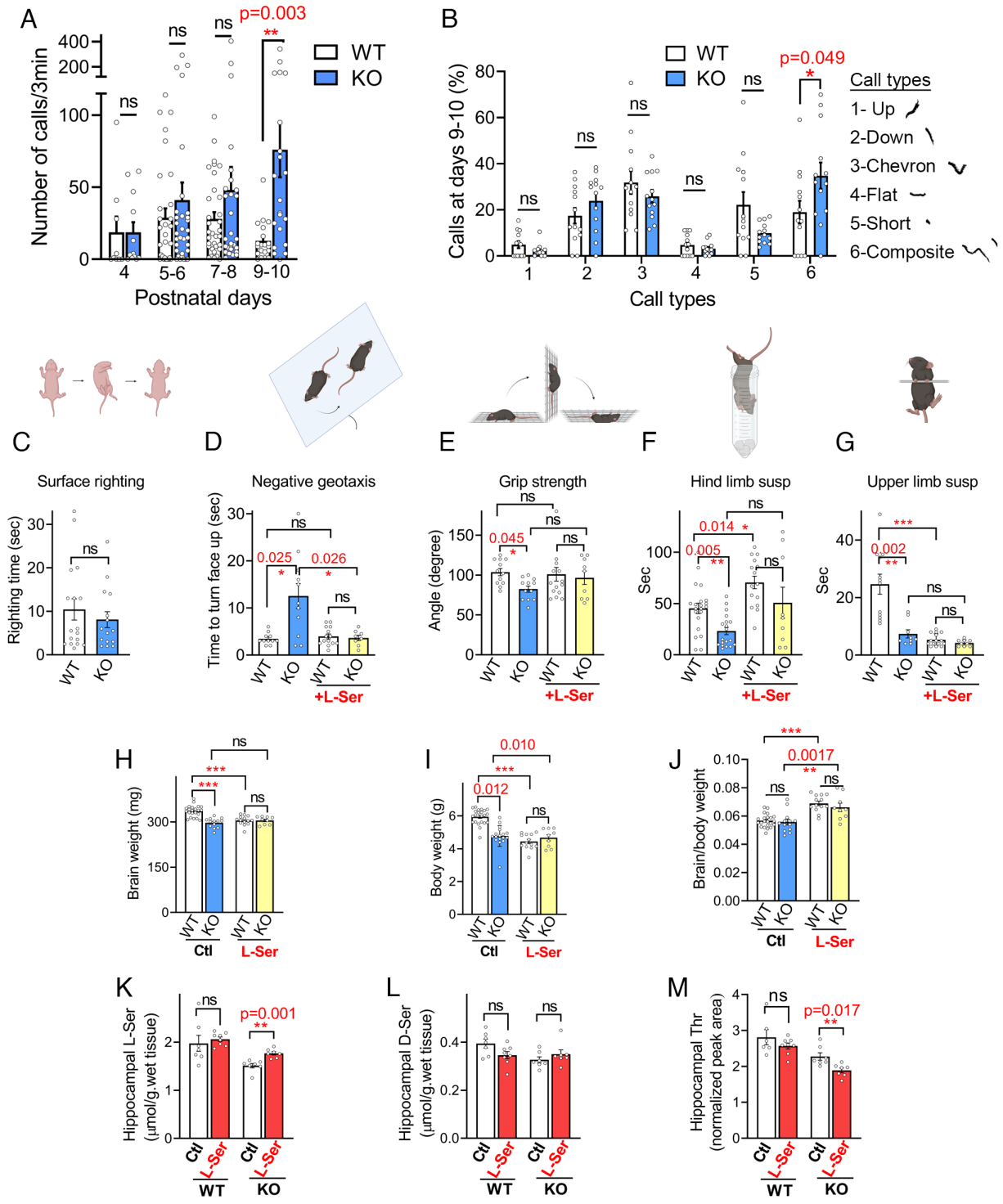

Fig. 8. Slc38a5-KO mice exhibit behavioral impairments and lower brain weight that are affected by perinatal L-serine administration. (*A*) Frequency of ultrasonic vocalizations recorded after separating the pups from the dam and litter. Data are means ± SEM of 9–32 mice/group. Kruskal–Wallis test with Dunn's multiple comparison test. (*B*) Classification of ultrasonic call types at P9–P10. Data are means ± SEM of 18–20 mice/group. Kruskal–Wallis test with Dunn's multiple comparison test. (*C*) Righting reflex of WT and Slc38a5-KO mice at P5. Data are means ± SEM of 18 (WT) and 15 (KO) mice. (*D*) Slc38a5-KO mice (P11) show impaired negative geotaxis, which is prevented by perinatal L-serine administration to the dam (8 g/L in the water). Data are means ± SEM of 8–14 mice/group. Brown Forsythe and Welch ANOVA test and Dunnett's T3 multiple comparisons test. (*E*) Slc38a5-KO mice (P11) show reduced grip strength but not after L-serine administration. Data are means ± SEM of 8–14 mice/group. Kruskal–Wallis test and Dunn's multiple comparisons test. (*F*) Slc38a5-KO mice (P11) display lower latency to fall in the hindlimb suspension test but not after L-serine administration. Data are means ± SEM of 8–21 mice/group. Brown Forsythe and Welch ANOVA test and Dunnett's T3 multiple comparisons test. (*G*) Slc38a5-KO mice (P11) exhibit lower latency to fall in the front limb suspension test. Data are means ± SEM of 8–14 mice/group. Brown Forsythe and Welch ANOVA test and Dunnett's T3 multiple comparisons test. (*H* and *I*) Brain (*H*) and body (*I*) weight in P11 WT and Slc38a5-KO with and without L-serine supplementation. Data are means ± SEM of 9–22 mice/group. The data on naive P11 mice in H and I were replotted from Fig. 1 *O* and *P*. One-way ANOVA and Sidak's multiple comparisons test. (*J*) L-Ser-treated WT and Slc38a5-KO mice display increased brain/body weight. One way ANOVA with Sidak multiple comparisons test. (*K–M*) Perinatal L-serine supplementation increased hippocampal L-serine (*K*) but not D-serine (*L*) in P11 Slc38a5-KO mice. Brain levels of threonine (*M*) decreased significantly after L-serine supplementation in P11 Slc38a5-KO mice. Data on naive P11 mice in *J* and *K* were replotted from Fig. 2 *A* and *B*. Data are means ± SEM of 7–8 mice/group. Student's *t* test. *P* values were adjusted for multiple comparisons using Bonferroni's method.

We believe that our constitutive Slc38a5-KO model is suitable for studying brain phenotypes because 1) Slc38a5 is 40 to 6,000 times more abundant in brain vessels than in peripheral blood vessels (11) and we found the transporter to be exclusively expressed in brain microvessels. 2) Slc38a5-KO mice had normal brain vessel development and did not exhibit changes in the general permeability of the BBB 3) Slc38a5 deletion did not affect serum or liver amino acids, suggesting lack of significant effects on peripheral tissues.

Our results show that L-serine uptake by the BBB is 10-fold higher in young mice compared with older mice. This is probably due, at least in part, to the transient expression of Slc38a5 in endothelial cells, where it is present in greater abundance in the abluminal (brain-facing) membranes. Such asymmetric localization will enable vectorial transport by increasing the efficiency of the flow of serine from the endothelial cell cytosol to the brain compartment.

Slc38a5 was thought to use glutamine and glycine as substrates (12). However, these properties have only been studied in vitro. In contrast, our *observations* indicate that Slc38a5 is a preferential serine transporter at the BBB because of the following: 1) Brain levels of glutamine and glycine did not change in the Slc38a5-KO mice. 2) The affinity of Slc38a5 for serine is 5 and 50 times higher than for glutamine and glycine, respectively. 2) Slc38a5-KO mice have lower transport of L-serine in vivo through the BBB. 3) Acute in vivo inhibition of Slc38a5 decreased brain L-serine and D-serine levels within 2.5 h but not L-glutamine levels. In view of this, we conclude that L-serine is the primary physiological Slc38a5 substrate at the BBB, rather than glutamine or glycine. However, our data do not exclude the possibility that other amino acids may be Slc38a5 substrates in other tissues (13).

Although threonine levels are lower in the brains of Slc38a5-KO mice, we found that threonine is a poor substrate for Slc38a5 and not transported by Slc38a5 in vivo. The improvement of the motor phenotype of Slc38a5-KO mice by L-serine did not restore threonine levels, which decreased even further. Of note, serine deficiency caused by deletion of Phgdh in mice also decreases brain threonine levels (24). On the other hand, Slc38a5-KO mice exhibited an increase in P2G, a glycolytic intermediate that is an activator of Phgdh (25). Additional studies will be required to elucidate the mechanisms underlying the changes in threonine and P2G in Slc38a5-KO mice.

Slc38a5-KO mice had lower levels of brain D-serine. However, it is unlikely that Slc38a5 physiologically imports D-serine directly from the blood. The plasma concentration of D-serine (~2 μM) is three orders of magnitude lower than the apparent affinity of Slc38a5 for D-serine (Km = 3.2 mM). The decrease in D-serine is likely due to the decreased availability of L-serine. Brain L-serine concentration (~1.4 mM) (5) is far below the saturation of serine racemase (Km = 10 mM) (26), so that a decrease in L-serine supply would result in a linear decrease in D-serine production rate. Other serine-consuming enzymes such as seryl-tRNA synthetase (Km = 7 μM) (27) and serine hydroxymethyl transferases (Km = 100–280 μM) (28) are likely to be saturated at physiologic L-serine levels. This could explain why the reduction of L-serine in Slc38a5-KO mice had no effect on translational control proteins or glycine synthesis.

Accumulation of doxSLs is implicated in peripheral neuropathy (17, 18) and macular disease (29). Both serine enantiomers promote synapse formation and increase dendritic spines number (2, 30). The increase in doxSLs along with the decrease in L-serine and D-serine in Slc38a5-KO mice may work together to alter synapse development, promote mitochondrial abnormalities, and decrease the postnatal neurogenesis at the DG.

In addition to the decrease in active zone and postsynaptic density area, Slc38a5-KO mice exhibited an apparent increase in the number of symmetric synapses, which are generally considered to be inhibitory. The proportion of synapses with asymmetric and symmetric contacts varies at different ages, with symmetric contacts predominating in P4–P11 and asymmetric in older rodents (19). The higher number of symmetric synapses exhibited in Slc38a5-KO mice is compatible with a neurodevelopmental delay.

Slc38a5-KO mice exhibited elevated USVs and motor impairments. L-serine supplementation improved some motor impairments in SLC38a5. Nevertheless, L-serine also improved the performance of WT in the hindlimb suspension test and affected brain and body weight, so it is likely that L-serine has a general effect on both genotypes. On the other hand, D-serine supplementation proved ineffective. These findings indicate that the observed deficits in Slc38a5-KO mice cannot be solely attributed to low D-serine levels. Our study underscores the key role of blood-derived L-serine in neurodevelopment and the importance of this new serine metabolic pathway predominantly found in young mice.

Materials and Methods

Experimental Model. $Slc38a5^{tm1\ (KOMP)\ Vlcg}$ mice (Slc38a5-KO) were obtained from KOMP Repository (UC Davis, Davis, CA) on a C57Bl/6 genetic background and back-crossed with C57BL/6J mice for five generations in our facility. All experiments were approved by the Animal Ethics Committee of the Technion.

In Vivo Uptake of Amino Acids via the Blood–Brain Barrier. Mice at (P11–P13) were anesthetized, and their thorax was opened. A microsyringe was prefilled with 5 μL of a mix of ^{3}H and ^{14}C isotopes and introduced into the heart apex, and the mix was injected quickly. Ten seconds after injection, the right atrium was cut, and the animal was quickly perfused with 4 mL of ice-cold PBS through the heart, and the brain and kidneys were harvested. Tissues were grinded in 1 mL of 0.1 M HCl, centrifuged for 10 min at 16,000 × g, and the supernatant was added to scintillation vials. Determination of ^{3}H was performed in a 0–11.5 keV window, while ^{14}C was measured at 35–156 keV. The contribution of ^{14}C to the ^{3}H counts was calculated and subtracted from each sample. Extraction fraction (EF) was defined as (CPM in the brain)/(CPM injected). To normalize for differences in cardiac output, the EF of each amino acid was divided by the EF of non-Slc38a5 substrates that were coinjected.

Additional materials and methods are described in the *SI Appendix, Methods*.

Data, Materials, and Software Availability. All study data are included in the article and/or supporting information.

ACKNOWLEDGMENTS. We thank Dr. Galit Saar for expert MRI acquisition and analysis and Maya Holdengreber for the help with confocal microscopy and image analysis. This work was funded by the Israel Science Foundation Grant 337/19, Allen and Jewell Prince Center for Neurodegenerative Diseases, Israel Ministry of Health (H.W.), and Russell Berrie Nanotechnology Institute (H.W. and A.A.). We thank Ms. Ifat Abramovich for her invaluable help in identifying metabolites in metabolomic experiments.

Author affiliations: [a]Department of Biochemistry, B. Rappaport Faculty of Medicine, Technion-Israel Institue of Technology, Haifa 3109601, Israel; [b]Department of Occupational Therapy, Faculty of Social Welfare and Health Sciences, University of Haifa, Haifa 3498838, Israel; [c]Electron Microscopy Unit, B. Rappaport Faculty of Medicine, Technion-Israel Institute of Technology, Haifa 3109601, Israel; [d]Department of Biotechnology and Life Sciences, Faculty of Biotechnology and Life Sciences, Sojo University, Kumamoto 860-0082, Japan; [e]Laboratory of Molecular Psychiatry, RIKEN Center for Brain Science, Saitama 351-0198, Japan; [f]Laura and Isaac Perlmutter Metabolomics Center, B. Rappaport Faculty of Medicine, Technion-Israel Institute of Technology, Haifa 3109601, Israel; [g]Department of Cell Biology and Biochemistry, University of Texas Southwestern Medical Center, Dallas, TX 75390-9039; [h]Sonoworx Co., Haifa 3473113, Israel; and [i]Technion-Integrated Cancer Center, B. Rappaport Faculty of Medicine, Technion-Israel Institute of Technology, Haifa 3109601, Israel

1. T. J. de Koning *et al.*, L-serine in disease and development. *Biochem. J.* **371**, 653–661 (2003).
2. S. Furuya *et al.*, L-serine and glycine serve as major astroglia-derived trophic factors for cerebellar Purkinje neurons. *Proc. Natl. Acad. Sci. U.S.A.* **97**, 11528–11533 (2000).
3. N. Damseh *et al.*, Mutations in SLC1A4, encoding the brain serine transporter, are associated with developmental delay, microcephaly and hypomyelination. *J. Med. Genet.* **52**, 541–547 (2015).
4. H. Wolosker, D. T. Balu, J. T. Coyle, The rise and fall of the d-serine-mediated gliotransmission hypothesis. *Trends Neurosci.* **39**, 712–721 (2016).
5. S. Neame *et al.*, The NMDA receptor activation by d-serine and glycine is controlled by an astrocytic Phgdh-dependent serine shuttle. *Proc. Natl. Acad. Sci. U.S.A.* **116**, 20736–20742 (2019).
6. M. Le Bail *et al.*, Identity of the NMDA receptor coagonist is synapse specific and developmentally regulated in the hippocampus. *Proc. Natl. Acad. Sci. U.S.A.* **112**, E204–E213 (2015).
7. B. Ngo *et al.*, Limited environmental serine and glycine confer brain metastasis sensitivity to PHGDH Inhibition. *Cancer Discovery* **10**, 1352–1373 (2020).
8. C. W. Kuzawa *et al.*, Metabolic costs and evolutionary implications of human brain development. *Proc. Natl. Acad. Sci. U.S.A.* **111**, 13010–13015 (2014).
9. D. C. Tarlungeanu *et al.*, Impaired amino acid transport at the blood brain barrier is a cause of autism spectrum disorder. *Cell* **167**, 1481–1494.e18 (2016).
10. Y. Pikman *et al.*, Targeting serine hydroxymethyltransferases 1 and 2 for T-cell acute lymphoblastic leukemia therapy. *Leukemia* **36**, 348–360 (2022).
11. R. N. Munji *et al.*, Profiling the mouse brain endothelial transcriptome in health and disease models reveals a core blood-brain barrier dysfunction module. *Nat. Neurosci.* **22**, 1892–1902 (2019).
12. E. H. Hamdani, M. Gudbrandsen, M. Bjorkmo, F. A. Chaudhry, The system N transporter SN2 doubles as a transmitter precursor furnisher and a potential regulator of NMDA receptors. *Glia* **60**, 1671–1683 (2012).
13. J. Kim *et al.*, Amino acid transporter Slc38a5 controls glucagon receptor inhibition-induced pancreatic alpha cell hyperplasia in mice. *Cell Metab.* **25**, 1348–1361.e8 (2017).
14. E. H. Finn, C. L. Smith, J. Rodriguez, A. Sidow, J. C. Baker, Maternal bias and escape from X chromosome imprinting in the midgestation mouse placenta. *Dev. Biol.* **390**, 80–92 (2014).
15. T. Nakanishi *et al.*, Structure, function, and tissue expression pattern of human SN2, a subtype of the amino acid transport system N. *Biochem. Biophys. Res. Commun.* **281**, 1343–1348 (2001).
16. Z. Wang *et al.*, Amino acid transporter SLC38A5 regulates developmental and pathological retinal angiogenesis. *ELife* **11**, e73105 (2022).
17. I. Alecu *et al.*, Localization of 1-deoxysphingolipids to mitochondria induces mitochondrial dysfunction. *J. Lipid Res.* **58**, 42–59 (2017).
18. A. Penno *et al.*, Hereditary sensory neuropathy type 1 is caused by the accumulation of two neurotoxic sphingolipids. *J. Biol. Chem.* **285**, 11178–11187 (2010).
19. B. Crain, C. Cotman, D. Taylor, G. Lynch, A quantitative electron microscopic study of synaptogenesis in the dentate gyrus of the rat. *Brain Res.* **63**, 195–204 (1973).
20. S. Han, Y. Y. Jeong, P. Sheshadri, X. Su, Q. Cai, Mitophagy regulates integrity of mitochondria at synapses and is critical for synaptic maintenance. *EMBO Rep.* **21**, e49801 (2020).
21. S. Sultan, E. G. Gebara, K. Moullec, N. Toni, D-serine increases adult hippocampal neurogenesis. *Front. Neurosci.* **7**, 155 (2013).
22. E. A. Mathews *et al.*, A distinctive layering pattern of mouse dentate granule cells is generated by developmental and adult neurogenesis. *J. Comp. Neurol.* **518**, 4479–4490 (2010).
23. S. Nagamachi *et al.*, Dietary L-serine modifies free amino acid composition of maternal milk and lowers the body weight of the offspring in mice. *J. Veterinary Med. Sci.* **80**, 235–241 (2018).
24. J. H. Yang *et al.*, Brain-specific Phgdh deletion reveals a pivotal role for L-serine biosynthesis in controlling the level of D-serine, an N-methyl-D-aspartate receptor co-agonist, in adult brain. *J. Biol. Chem.* **285**, 41380–41390 (2010).
25. T. Hitosugi *et al.*, Phosphoglycerate mutase 1 coordinates glycolysis and biosynthesis to promote tumor growth. *Cancer Cell* **22**, 585–600 (2012).
26. V. N. Foltyn *et al.*, Serine racemase modulates intracellular D-serine levels through an alpha, beta-elimination activity. *J. Biol. Chem.* **280**, 1754–1763 (2005).
27. K. M. Holman, A. K. Puppala, J. W. Lee, H. Lee, M. Simonovic, Insights into substrate promiscuity of human seryl-tRNA synthetase. *RNA* **23**, 1685–1699 (2017).
28. G. Giardina *et al.*, How pyridoxal 5′-phosphate differentially regulates human cytosolic and mitochondrial serine hydroxymethyltransferase oligomeric state. *FEBS J.* **282**, 1225–1241 (2015).
29. M. L. Gantner *et al.*, Serine and lipid metabolism in macular disease and peripheral neuropathy. *N Engl. J. Med.* **381**, 1422–1433 (2019).
30. D. K. Park *et al.*, Reduced d-serine levels drive enhanced non-ionotropic NMDA receptor signaling and destabilization of dendritic spines in a mouse model for studying schizophrenia. *Neurobiol. Dis.* **170**, 105772 (2022).